DETERMINATION OF MICROCRACK BOUNDARY RESULTING FROM ROCK BLASTING WITH SEISMIC TRAVELTIME TOMOGRAPHY①

Zhang Jichun
Department of Underground Eng and Geotechnical Eng, Southwest Jiaotong University, Chengdu 610031, P. R. China
Song Linping
Institute of Acoustics and Lab of Modern Acoustics, Nanjing University, Nanjing 210093, P. R. China

ABSTRACT Combining the crosshole elastic wave survey with the seismic traveltime tomography, a new method to determine the microcrack zone boundary of rock masses blasting was proposed. The method of ray tracing of slowness square was briefly introduced which was used to calculate the coefficients of traveltime equations, then the weighted least-square solution of solving the large sparse linear equations and its commonly used iterative procedure were given. Based on the data of P-wave traveltime measured in six small-charge blasting experiments at Sanxia dam, the P-wave velocity distributions of rock mass before and after blasting are reconstructed and all of the microcrack depths and microcracking zone diameters in rock masses resulting from blasting were finally determined. The further research works find that the microcrack depth is much smaller than the microcracking zone radius and they almost linearly increase with the addition of charge quantity, moreover, the increment of microcrack depth is much greater than that of microcracking zone radius.

Key words rock mass blasting microcracking zone measuring method tomography

1 INTRODUCTION

The measurement of the microcracking zone resulting from rock mass blasting (the adjacent region between fragmented zone and elastic zone) is one of the important technical problems being studied in the field of engineering blasting and rock mechanics. The accurate measurement of microcrack boundary not only can provide a reliable basis for reasonably selecting the parameters of excavating blasts in hydraulic engineering, underground structure engineering and tunneling engineering, but also contributes to correctly evaluating the damage degrees of surrounding rock, bed rock and rock slope resulting from blasting effects and, moreover, determining the method of rock protection and its parameters economically and reasonably.

The measurement of microcracking zone can be generally classified as absolute observation and relative observation. The absolute observation is to investigate the region of blasted cracks through drilling or measuring the parameters of rock mass such as rate of cracks, infiltration of water and vibration velocity of particles in blasting, by which the breakage zone of rock mass can be assessed. Only can the rough scope of microcracking zone be measured qualitatively using this sort of method while its boundary can not be determined. The relative observation is to compare the variation of elastic wave velocities or sound-energy absorption coefficients of rock mass before and after blasting and determine the fracture scope of rock mass blasting. This sort of method, however, is restricted by means of data processing and analyzing, its measured results

① Project 2980 supported by China Postdoctoral Science Foundation Received Jul. 19, 1996; accepted Oct. 13, 1997

are low precision; besides, owing to using the observation of horizontal transmission mostly, the microcrack depth below the bottom of blasthole can be merely obtained and the boundary of microcracking zone in rock blasting can not be measured yet. If improving the accuracy of measuring the microcrack boundary, therefore, it is necessary that a new efficient method of data processing and analyzing should be found.

In early 1980s, the technique of seismic tomography was rapidly developed and widely used in geophysical exploration. John and Wong *et al* deduced the geologic structures between bore holes and obtained the corresponding velocity field of seismic waves by means of crosshole transmission tomography[1, 2]. In recent years the theoretical and applied research works on seismic tomography have been systematically and thoroughly carried out in our country. Moreover, the seismic tomography technique had been tentatively applied to the constructions of Ertan hydraulic engineering, Qingjiang-Ge Heyan engineering and Xin Anjiang power station. This technique can more accurately circle the weak mudrock belt within bed rock and also inspect and evaluate the quality of heavy-curtain grouting[3-5]. With the gradual development of both the various kinds of ray tracing algorithm and the solutions of large sparse linear equations, the precision of seismic tomography is greatly improved[6-7], which makes it possible that the microcrack boundary of rock mass is more exactly circled by comparing the difference between the velocity distributions before and after blasting. Based on the data of P-wave traveltime measured before and after field blasting, the accurate measurement of the boundary of microcracking zone created in rock mass blasting is accomplished in this paper by using the algorithm of ray tracing of slowness square and the weighted least square solution.

2 FUNDAMENTAL MODEL OF SEISMIC TRAVELTIME TOMOGRAPHY AND ITS ALGORITHM

Blasting effect results in rock mass breaking and microcracking in a finite region, which causes the decrease of P-wave velocity in this region. But for undamaged rock mass after blasting, its velocity is the same as that before blasting. For this reason, the fundamental viewpoint of determining the boundary of microcrack zone for blasting in rock mass through seismic tomography is: to measure the P-wave traveltime in rock mass before and after blasting in different orientation using the crosshole seismic waves survey; to do inverse calculation applying the technique of seismic traveltime tomography; to obtain the distributions of P-wave velocity in rock mass before and after blasting and determine the microcrack boundary by comparing these two velocity distributions.

2.1 Traveltime equations

The propagating velocity of seismic waves varies with the different regions because rock mass is heterogeneous irrespective of before and after blasting, therefore, the traveltime of seismic ray between two observation holes is equal to the accumulation of the traveltime of P-wave propagating in each rock element. For a 3-D geophysical model, the traveltime of seismic ray is a function of both the velocity and the ray path geometry. Assume $u(\boldsymbol{r})$ is slowness(reciprocal of velocity) function and $\boldsymbol{r}$ position vector, the traveltime of seismic ray is given by

$$t = \int_{\Gamma} u(\boldsymbol{r})\,\mathrm{d}s \qquad (1)$$

where Γ—the ray path of seismic waves; $\mathrm{d}s$—the element of arc length along the ray.

Because $u(\boldsymbol{r})$ is implicated in the ray path Γ, the relation between traveltime and slowness function is highly nonlinear. It can be known from Fermat's principle that the traveltime of a ray is stationary for small shifts of the ray location. Therefore, a linear relation is derived by replacing the unknown ray path in Eqn. (1) with the ray path Γ^0 in reference model as follows:

$$t = \int_{\Gamma^0} u(\boldsymbol{r})\,\mathrm{d}s \qquad (2)$$

In 2-D ray tomography procedure, the target plane is discretized into a set of rectangular cells or pixels, with u_j denoting the slowness value of the jth grid point of cells, $j = 1 \sim n$. Then the slowness at any point of the model can

be interpolated with a proper basis function. Taking a first-order B-spline as the basis function $\alpha_j(\boldsymbol{r})$, Eqn. (2) is transformed into[8]

$$t = \sum_{j=1}^{n}\left[\int_{\Gamma_1^0}\alpha_j(\boldsymbol{r})\,\mathrm{d}s\right]u_j \tag{3}$$

Suppose the observation values of traveltime for m seismic rays is t_i, $i = 1 \sim m$, the linear equations of seismic traveltime can be obtained from Eqn. (3) as

$$\boldsymbol{t} = \boldsymbol{A}\boldsymbol{u} \tag{4}$$

where $\boldsymbol{t}$ —the traveltime column vector of dimension m; $\boldsymbol{u}$ —model slowness column vector of dimension n; $\boldsymbol{A}$ —$m \times n$ matrix whose elements a_{ij} is determined by the integral of basis function $\alpha_j(\boldsymbol{r})$ along the ray path Γ_1^0 through ray tracing at current model.

2.2 Model of ray tracing for square of slowness

According to ray theory, seismic ray obeys the following second-order ordinary differential equation[9]

$$\frac{\mathrm{d}}{\mathrm{d}s}\left(u\frac{\mathrm{d}\boldsymbol{r}}{\mathrm{d}s}\right) = \nabla(u) \tag{5}$$

where ∇ —gradient operator; s —the arc length for ray parameter.

Set $u\,\mathrm{d}\sigma = \mathrm{d}s$, Eqn. (5) can be rewritten as

$$\frac{\mathrm{d}^2\boldsymbol{r}}{\mathrm{d}\sigma^2} = \frac{1}{2}\nabla(u^2) \tag{6}$$

where u^2 —the square of slowness. Assume the distribution of the square of slowness is linear and the relation between ray parameter s and σ is taken into account, the exact expressions on the trajectory, direction and traveltime of a ray propagation can be obtained[10]:

$$\left.\begin{aligned}\boldsymbol{r} &= \lambda\sigma^2/4 + \boldsymbol{p}_0\sigma + \boldsymbol{r}_0\\ \boldsymbol{p} &= \lambda\sigma/2 + \boldsymbol{p}_0\\ t &= \lambda\sigma^3/12 + \lambda\boldsymbol{p}_0\sigma^2/2 + \boldsymbol{p}_0\boldsymbol{r}_0\sigma + u_0^2\sigma\end{aligned}\right\} \tag{7}$$

where λ—gradient vector of the square of slowness, $\boldsymbol{r}_0$ and $\boldsymbol{p}_0$ are the position vector and slowness vector at the reference point respectively.

The paraxial ray method is used to perform ray tracing between the two point. Defining the position and slowness vectors of a paraxial ray as: $\boldsymbol{r} = \boldsymbol{r}_0 + \delta\boldsymbol{r}$, $\boldsymbol{p} = \boldsymbol{p}_0 + \delta\boldsymbol{p}$, and introducing the Hamiltonian $H = (p^2 - u^2)/2$ into Eqn. (6), the analytical solution of the paraxial ray equations is derived based on the linear square of slowness function:

$$\left.\begin{aligned}\delta\boldsymbol{r} &= \delta\boldsymbol{p}_0\sigma + \delta\boldsymbol{r}_0\\ \delta\boldsymbol{p} &= \delta\boldsymbol{p}_0\end{aligned}\right\} \tag{8}$$

additionally, there is a constraining condition

$$\boldsymbol{p}_0 \cdot \delta\boldsymbol{p} = \lambda \cdot \delta r/2 \tag{9}$$

The problem of the two-point ray tracing is analytically solved from Eqn. (7) and Eqn. (8), which gives the values of the elements in matrix $\boldsymbol{A}$.

2.3 Weighted least square solution

The large scale sparse system of linear Eqn. (4) is solved by minimizing the following quadratic function

$$\varphi(\boldsymbol{u}) = (\boldsymbol{A}\boldsymbol{u} - \boldsymbol{t})^{\mathrm{T}}\boldsymbol{W}_1(\boldsymbol{A}\boldsymbol{u} - \boldsymbol{t}) + \mu(\boldsymbol{u} - \boldsymbol{u}_0)^{\mathrm{T}}\boldsymbol{W}_2(\boldsymbol{u} - \boldsymbol{u}_0) \tag{10}$$

where $\boldsymbol{W}_1$ and $\boldsymbol{W}_2$ —$m \times m$, $n \times n$ real symmetry weighting matrixes for data and model, respectively; $\boldsymbol{u}_0$ —reference model vector; μ —damping factor, which determines the relative importance of the two terms at the right side of Eqn. (10).

The normal equation resulting from Eqn. (10) is

$$(\boldsymbol{A}^{\mathrm{T}}\boldsymbol{W}_1\boldsymbol{A} + \mu\boldsymbol{W}_2)(\boldsymbol{u} - \boldsymbol{u}_0) = \boldsymbol{A}^{\mathrm{T}}\boldsymbol{W}_1(\boldsymbol{t} - \boldsymbol{A}\boldsymbol{u}_0) \tag{11}$$

Through analyzing the generalized eigenvalue problem, the weighting matrixes proposed by Berryman in cell model can also be extended to those of the grid model[11]

$$\boldsymbol{W}_1 = \boldsymbol{C}^{-1} \tag{12}$$

$$\boldsymbol{W}_2 = \boldsymbol{D} \tag{13}$$

where $\boldsymbol{C}$ and $\boldsymbol{D}$ —the diagonal matrixes whose elements are respectively given by

$$c_{ii} = \sum_{j=1}^{n} a_{ij}u_j \quad (1 \leqslant i \leqslant m) \tag{14}$$

$$d_{jj} = \sum_{i=1}^{m} a_{ij}/u_j \quad (1 \leqslant j \leqslant n) \tag{15}$$

The element c_{ii} is the estimated traveltime of ith ray at the current model and the element d_{jj} is the total contribution of the associated rays to the jth grid point. For the shorter ray paths which more probably stay in the imaging plane, the corresponding signal-noise ratios are generally higher, thus more importance are assigned to

the ray path with small traveltime in Eqn. (12). In addition, the denser the rays are, the more accurate the reconstructed image is, therefore, Eqn. (13) emphasizes the importance of the cell which is traversed by many rays.

2.4 Reconstruction algorithm

The methods of algebraic reconstruction technique(ART), simultaneous iterative reconstruction technique (SIRT) and conjugate gradient(CG) are commonly used to solve the large scale sparse system of linear equations. To speed up the convergence of the iterative solution and save the computer memory, the CG algorithm is applied to finding the solution of the weighted least square problem in Eqn. (10) according to the following steps:

$$\boldsymbol{x}_0 = 0$$

$$\boldsymbol{r}_0 = \boldsymbol{p}_0 = \boldsymbol{A}^{\mathrm{T}} W_1 (\boldsymbol{t} - \boldsymbol{A}\boldsymbol{u}_0)$$

For $k = 0, 1, 2, \cdots$

$$\boldsymbol{s}_k = \boldsymbol{A}\boldsymbol{p}_k$$

$$\alpha_k = (\boldsymbol{r}_k, \boldsymbol{r}_k) / \{\mu[(\boldsymbol{p}_k, W_2\boldsymbol{p}_k) + (\boldsymbol{s}_k, W_1\boldsymbol{s}_k)]\}$$

$$\boldsymbol{x}_{k+1} = \boldsymbol{x}_k + \alpha_k \boldsymbol{p}_k$$

$$\boldsymbol{u}_{k+1} = \boldsymbol{u}_0 + \boldsymbol{x}_{k+1}$$

$$\boldsymbol{r}_{k+1} = \boldsymbol{r}_k - \alpha_k [\mu W_2 \boldsymbol{p}_k + \boldsymbol{A}^{\mathrm{T}} W_1 \boldsymbol{s}_k]$$

If $\boldsymbol{r}_{k+1} = 0$ then quit

$$\beta_k = (\boldsymbol{r}_{k+1}, \boldsymbol{r}_{k+1}) / (\boldsymbol{r}, \boldsymbol{r}_k)$$

$$\boldsymbol{p}_{k+1} = \boldsymbol{r}_{k+1} + \beta_k \boldsymbol{p}_k$$

where α_k and β_k —real numbers; the others are vectors or matrixes.

3 APPLICATION AND ANALYSIS

3.1 Measuring method of field experiment

The field experiments have been done at the bottom of weak weathering granite in temporary ship lock 119.4 m above sea level on the left bank of the Sanxia Project. The 12 sets of traveltime data before and after blasting for 6 small-charge experiments are obtained by using the crosshole transmission survey. The distance between the emission hole of vibration source and the receiving hole is 8 m and the depth of these holes is 2.2 to 2.6 m. The blasting hole is located at the center of the corresponding emission and receiving holes, and its depth is 1.7 to 2.2 m.

The observation system of crosshole seismic waves is shown in Fig. 1. First of all, placing the emitter at the first point of excitation in field measurement, the P-wave form is successively recorded from the first receiving point to the last one; and then moving the emitter to the next point of excitation, the values of P-wave traveltime from this emitting point to all of the receiving points are measured until the values of P-wave traveltime from all of the emitting points to each of the receiving points (t_i) are obtained, here $i = 1 \sim m$. Thus the observation traveltime vector $\boldsymbol{t}$ of dimension m is formed. The distances between each of the emitting points or the receiving points are all 0.2 m in Fig. 1 and the emitting and receiving holes before and after blasting are the same.

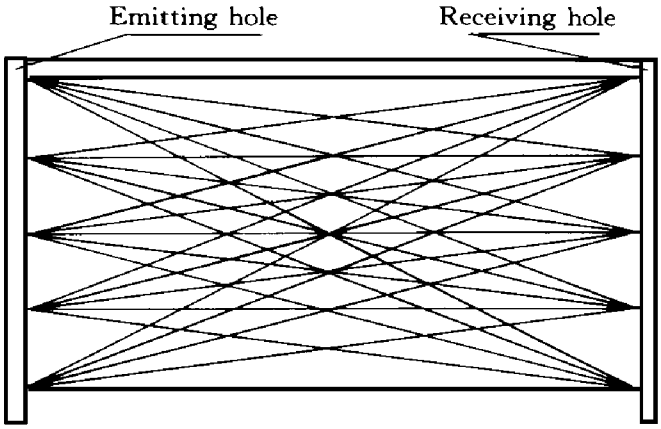

Fig. 1 The observation system of crosshole

3.2 Result of seismic tomography and its analysis

According to the observation system of crosshole seismic waves, the region of rock mass in blasting is discretized into the 0.2 m × 0.2 m imaging elements whose total number for each tomographic imaging is over 400. In addition, the initial models of reference are all considered as uniform ones and their velocities are equal to 3 600 m/s.

The grey tomographic images of the P-wave velocity distribution in rock mass before and after No. 1 blasting from tomographic images are shown in Fig. 2. Comparing Fig. 2(a) with Fig. 2(b), it can be found that in the imaging center

of velocity images, i. e. the region near the blasthole, the P-wave velocity in rock mass after blasting (less than 2 800 m/s) is obviously less than that before blasting (3 200~ 3 400 m/s), especially the region two (r_2) in Fig. 2(b); in the more distant region away from the blasthole, nevertheless, the P-wave velocities after blasting almost are the same as those before blasting. Thus, the clear boundary shaped like "V" is formed in the center of Fig. 2(b), which is defined as the boundary of microcracking zone in this paper. This boundary objectively differentiates between the regions of which the P-wave velocities have changed and unchanged. The other five reconstruction images of P-wave velocity before and after blasting all present the above-mentioned changing characteristics.

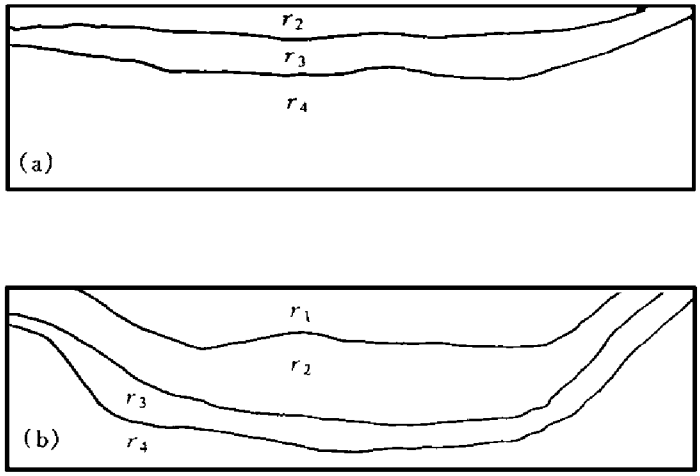

Fig. 2 The velocity distribution before and after No. 1 blasting

(a) —The velocity distribution before blasting; (b) —The velocity distribution after blasting

r_1 —v < 2 600 m/s; r_2 —v = 2 600~ 2 800 m/s; r_3 —v = 2 800~ 3 200 m/s; r_4 —v > 3 200 m/s

The boundary of microcracking zone for blasting may be determined according to a difference of P-wave velocities of imaging elements before and after blasting. Because the important data of selecting the parameters of rock mass blasting and determining the protection of surrounding rock as well as its reinforcing parameters are both the vertical microcrack depth and the horizontal microcracking zone radius which are given by using the bottom of blasthole as the datum point, the microcrack depth and microcraking zone radius of 6 experiments and their corresponding blast parameters are listed in Table 1. The blasthole diameter for experiments is 100mm and ammonium nitrate and fuel oil explosive (ANFO) is used for blasting.

It is known from Table 1 that the microcracking zone radius is greater than the microcrack depth in a blast and the ratio of these two parameters equals 4 to 8, which illustrates that the restrictive effect below the bottom of blasthole is much greater than that in the horizontal direction. When excavating the foundation pit of the dam, chamber and tunnel using the technique of short-hole blasting, therefore, the microcracking degree and its range caused by blasting effect in the direction at right angles to the blasthole axis must be fully taken into account so as to select charging parameters reasonably. The effective protecting measures should be taken especially bordering on the final scope, to reduce the microcracking effect of blasting upon rock mass.

Table 1 The dimension of microcracking zone and its corresponding blasting parameters

No	blasthole depth/ m	Charge /kg	Microcrack depth/ m	Microcracking zone radius/ m
1	1.8	1.0	0.3	1.4
2	1.8	1.4	0.4	1.7
3	1.7	0.8	0.2	1.6
4	2.2	1.2	0.3	1.7
5	1.8	1.8	0.5	1.8
6	2.0	2.6	0.7	2.0

The relations between the charge and the microcrack depth as well as the microcraking zone radius are shown in Fig. 3 and Fig. 4, respectively. With reference to these two charts it is clear that both the microcrack depth and the microcracking zone radius increase almost directly as the charge increases and, moreover, the incremental range of the microcrack depth (250%) is much greater than that of the microcracking zone radius (42%). For these reasons, while excavating rock mass bordering on the foundation bed of dam, the charging quantity of a blasthole must be controlled and the excavating

method of large-charge or concentrated-charge blasting is used as little as possible or not used so as to prevent the microcrack depth of bed rock from much deepening.

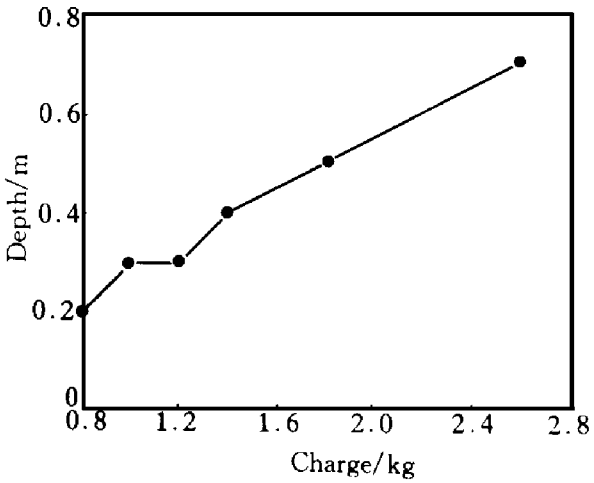

Fig. 3 The relation between microcrack depth and charge

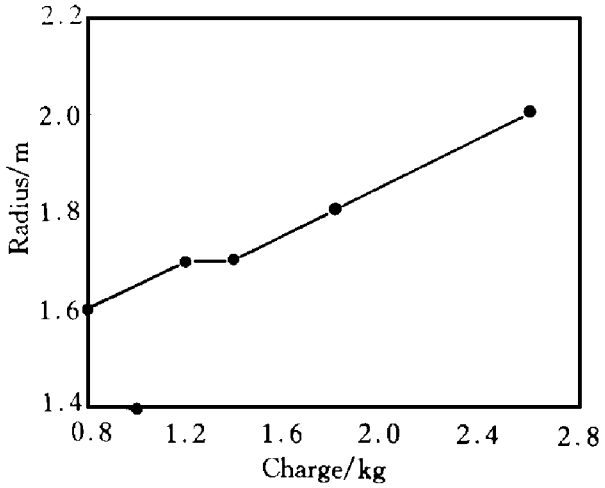

Fig. 4 The relation between microcracking zone radius and charge

4 CONCLUSIONS

From the above studies, some important results can be obtained as follows:

(1) The P-wave velocity distributions in rock mass before and after excavating blast may be reconstructed by combining the crosshole seismic wave survey with the traveltime tomography, moreover, the boundary of microcracking zone resulting from blasting effect in rock mass can be more accurately determined.

(2) The trajectory, direction and traveltime of seismic wave propagation can be given by the model for ray tracing of the square of slowness which embodies the reflection, refraction and curvature in the process of P-wave propagation. The weighted least-square solution, through the different weights, reflects the effects of travel-time and density of rays on the reconstructed image, which effectively improve the imaging precision.

(3) In short-hole and small-charge blasting, the microcrack depth is much less than the microcracking zone radius and its value is merely about a sixth of the microcracking zone radius. If the diameter of a blasthole is constant, the microcrack depth and the microcracking zone radius resulting from blasting in rock mass almost directly increase with the increase of the charging quantity, furthermore, the incremental range of the microcrack depth is much greater than that of the microcracking zone radius.

REFERENCES

1 Peterson J E, Paulsson B N P and McEvilly T V. Geophysics, 1985, 50(10): 1566- 1580.
2 Wong J, Hurley P and West G F. Geophys Res Letter, 1983, 10(8): 686- 689.
3 Song Z Z *et al*. Eng Geophys Exploration, (in Chinese), 1990, (7): 1- 10.
4 Gao P F and Nie Y J. J Yangtze River Sci Res Institute, (in Chinese), 1992, 9(4): 33- 39.
5 Li Z M, Xiong Y H and Liu R Z. J Yangtze River Sci Res Institute, 1993, 10(3): 37- 43.
6 Vidale J E. Bull Seism Soc Am, 1988, (78): 2062- 2076.
7 Nolet G. J Comp phys, 1985, (61): 463- 482.
8 Song L P. Chinese J Comp Phys, (in Chinese), 1995, 12(4): 499- 504.
9 Nolet G. Seismic Tomography. Reidel Publishing Company, 1987: 1- 23.
10 Song L P *et al*. Comp Tech Geophys and Geochem Exploration, (in Chinese), 1993, 15(3): 238- 244.
11 Song L P. J Chengdu Institute Tech, (in Chinese), 1994, 21(1): 107- 113.
12 Frank M and Balanis C A. IEEE Trans Geosci Remote Sensing, 1989, (27): 339- 343.

(Edited by He Xuefeng)